AN EFFICIENT METHOD TO MODEL SEISMIC PROPAGATION IN DIFFUSIVE-VISCOUS MEDIA WITH DIPPING INTERFACES

FENGYUAN SUN, JINGHUAI GAO and NAIHAO LIU

School of Electronic and Information Engineering, Xi'an Jiaotong University, Xi'an 710049, P.R. China,
National Engineering Laboratory for Offshore Oil Exploration, Xi'an 710049, P.R.China. jhgao@mail.xjtu.edu.cn

(Received February 3, 2018; revised version accepted November 10, 2018)

ABSTRACT

Sun, F.Y., Gao, J.H. and Liu, N.H., 2019. An efficient method to model seismic propagation in diffusive-viscous media with dipping interfaces. *Journal of Seismic Exploration*, 28: 21-40.

Partial wavefield that is not be interfered by other waves plays a significant role in seismic exploration. In many applications, geophysicists are only interested in partial wavefields. In this work, we first derive an efficient workflow to simulate partial wavefields in the diffusive-viscous media with the presence of dipping layers. It can efficiently calculate various partial wavefields for investigating the seismic exploration based on the diffusive-viscous theory. Especially, the reflection/transmission coefficients in the dip layered media are studied through the coordinate transformation and the plane wave theory. Then, a fast integral method is used to synthesize the wavefields from a point source, and the best integral path is chosen to improve the accuracy and the computational efficiency. By choosing the appropriate sign of the complex slowness, the instability phenomenon in the computation process can be avoided. The analysis and numerical examples show that the proposed method is stable and efficient.

KEY WORDS: partial wavefield, layered diffusive-viscous media, reflectivity method.

INTRODUCTION

The complete seismic wavefield is usually complex because it contains many types of waves. However, when we study the phenomenon of frequency-dependent due to the presence of fluids, we are only interested in the partial wavefield which is not interfered by other waves. The seismic response in hydrocarbon reservoirs is affected by many factors, such as the

0963-0651/19/$5.00 © 2019 Geophysical Press Ltd.

porosity, permeability, viscosity and so on (Toksöz and Johnston, 1981; Raikes and White, 1984). Goloshubin et al. (1996) observed traveltime delay and energy redistribution when comparing cases of water-saturated and dry-sandstone rocks in both laboratory and field data. To explain the anomalies, Korneev et al. (2004) proposed the diffusive-viscous theory and showed the general link between characteristics of fluid saturation and seismic attenuation. In this paper, we propose a modeling method which combines the diffusive-viscous theory and the reflectivity method to simulate seismic wave propagation.

There are many other numerical modeling methods to compute complete seismic wavefield, such as the finite difference method (Alterman and Karal, 1968; Marfurt, 1984; Arntsen et al., 1998; Wu and Harris, 2004; Gao and Zhang, 2013; Han et al., 2014), finite element method (Smith, 1975; Peelamedu, 1999; Guo et al., 2001; Min, 2002; Taeyoung et al., 2009; Zhang and Li, 2013; Meng and Fu, 2017) and spectral element method (Patera, 1984). However, it is difficult to obtain accurate waves in many applications, which are not interfered especially in thin layers. As a result, geophysicists are only interested in partial wavefield. For example, the primary reflected waves are needed to study amplitude variations with offset (Shuey, 1985). In borehole geophysics, reflections are complex because downgoing-waves and upgoing-waves interfere with each other. The interference may affect the accuracy of seismic imaging (Mars, 1999; Nowak and Imhof, 2004; Serdyukov and Duchkov, 2015). For multiple predictions, we often focus on the multiples of target layers only (ten Kroode, 2002). The presence of interbed multiples has a strong impact on the interpretation, which distorts the wavelets of true reflections and reduces the quality of final images. Therefore, seismic simulation of wavefields without interbed multiples before imaging is often needed in practice (Wang et al., 2016). Therefore, modeling partial wavefields without interference is important.

To simulate partial wavefield and remove the interference errors, we propose a novel workflow based on the diffusive-viscous theory and the reflectivity method in this paper. The main advantage of the proposed method is its capacity to give both a total solution of wavefield and partial wavefield of interest in layered media. After decomposing all wave types into upgoing- and downgoing- waves, the proposed method describes seismic behavior in stratified earth models in a convenient way, where waves can be decoupled into different wave types. Reflections, transmissions and the corresponding multiples inside thin layers inserted between two half-spaces can be fully modeled, respectively.

Seismic wave propagation in stratified media has been studied for a long time (Aki and Richards, 2002). The method of seismogram synthesis that we will present is for multi-layered media with dipping interfaces. This method can be viewed as an extension of the reflectivity method for horizontal layered media to dipping layered media. And it can also be used for layered media with the horizontal interface. The accurate and stable result in dipping layered media is important in many practical applications

because dipping layers are more realistic than horizontal layers. The difference between horizontal and dipping layered media is that the slowness of the ray paths is not conserved in dipping layered media. Therefore, a complicated algorithm to model wave propagation in dipping layered media than that in horizontal layered media. There are also other approaches to simulate the wave propagation in a layered model with dipping interfaces. For instance, the wavefield extrapolation method can be used to simulate wave propagation in elastic media with dipping interfaces (Berkhout et al., 1982; Bourbie and Gonzalez-Serrano, 1983). The generalized reflectivity method proposed by Chen (1990, 1996) and boundary element approach of Ge and Chen (2007). Liu et al. (2008) were proposed to simulate wave propagation in stratified elastic media with irregular interfaces. However, these methods have various limitations for simulating partial wavefields. The extended reflectivity method of Zhao et al. (2017) can also be used to model wave propagation in dip-layered media, but there is not a discussion about the best integral path, and the computation process is unstable and the overflow phenomenon always occurs.

On the basis of previous works that have been referred earlier, we derive a stable and efficient partial wavefield simulation method in diffusive-viscous media based on the reflectivity method. Then, we simulate the propagation of diffusive-viscous waves in fluid-saturated layered models in the frequency-wavenumber domain. A fast integral method is used to synthesize the wavefield for a point source. Numerical examples and the comparison with the finite difference solution demonstrate that our proposed method is computationally and mathematically efficient.

DIFFUSIVE-VISCOUS WAVE EQUATION

The diffusive-viscous theory is proposed to explain the phenomenon that fluid-saturated layers generate large reflection amplitudes at low frequencies (Korneev et al., 2004). In the absence of a source term, the wave equation can be written as

$$\frac{\partial^2 u}{\partial t^2}+\gamma\frac{\partial u}{\partial t}-\eta\left(\frac{\partial^3 u}{\partial z^2\partial t}+\frac{\partial^3 u}{\partial x^2\partial t}\right)-v^2\left(\frac{\partial^2 u}{\partial x^2}+\frac{\partial^2 u}{\partial z^2}\right)=0 \quad , \tag{1}$$

where γ represents the diffusional dispersive force with a unit of Hz, η denotes the viscosity with a unit of m^2/s. These two variables are considered to be attenuation parameters, which are related to porosity and permeability. v is the velocity in a non-dispersive situation. u denotes the displacement.

The harmonic plane wave solution of eq. (1) is given by

$$u=\exp\left[j\omega t+j\omega\left(px+qz\right)\right]. \tag{2}$$

where ω denotes the angular frequency, p and q are the horizontal slowness and the vertical slowness, respectively,

$$p = \frac{1}{V}\sin(\varepsilon) \ ,$$

$$q = \sqrt{\frac{1}{V^2} - p^2}, \tag{3}$$

where V is the complex velocity, ε is the incident angle between the ray and the vertical direction. The complex velocity and the quality factor Q can be computed by (Carcione and Tinivella, 2001)

$$V = \sqrt{\frac{v^2 + i\eta\omega}{1 - i\dfrac{\gamma}{\omega}}} \ ,$$

$$Q = \frac{\mathrm{Re}\left(V^2\right)}{\mathrm{Im}\left(V^2\right)} = \frac{\left(v^2 - \eta\gamma\right)\omega}{\eta\omega^2 + \gamma v^2} \ . \tag{4}$$

Eq. (4) indicates that V and Q not only depend on the attenuation caused by the diffusive and viscous properties, but also on the frequency. The resulted velocity and wavenumber reduce to those of acoustic media when attenuation parameters approach to zero, whereas Q becomes infinity, i.e., no attenuation. The detailed derivation of eq. (4) can be seen in the Appendix.

REFLECTION AND TRANSMISSION AT A DIPPING INTERFACE

To determine the reflection and transmission coefficients at a dipping interface in layered diffusive-viscous media, two coordinate systems are introduced as shown in Fig. 1(a). The global coordinate system XOZ with X-axis at the horizontal direction. The local coordinate system $\hat{X}\hat{O}\hat{Z}$ with $\hat{X}$-axis at the dipping interface and its origin in XOZ system is (x_0, z_0). α is the plane wave velocity, ρ is the density. The subscript "1" and "2" denote upper and lower media, respectively. γ and η are the diffusive-viscous parameters. The variables with a superscript "$\wedge$" are in the local coordinate system. Otherwise, they are in the global coordinate system.

Two different coordinate systems in Fig. 1(a) can be transformed to each other by a rotation matrix $\mathbf{C}$,

$$\mathbf{C} = \begin{bmatrix} \cos\theta & \sin\theta \\ -\sin\theta & \cos\theta \end{bmatrix}, \quad \begin{bmatrix} \hat{x} \\ \hat{z} \end{bmatrix} = \mathbf{C}\begin{bmatrix} x - x_0 \\ z - z_0 \end{bmatrix}. \tag{5}$$

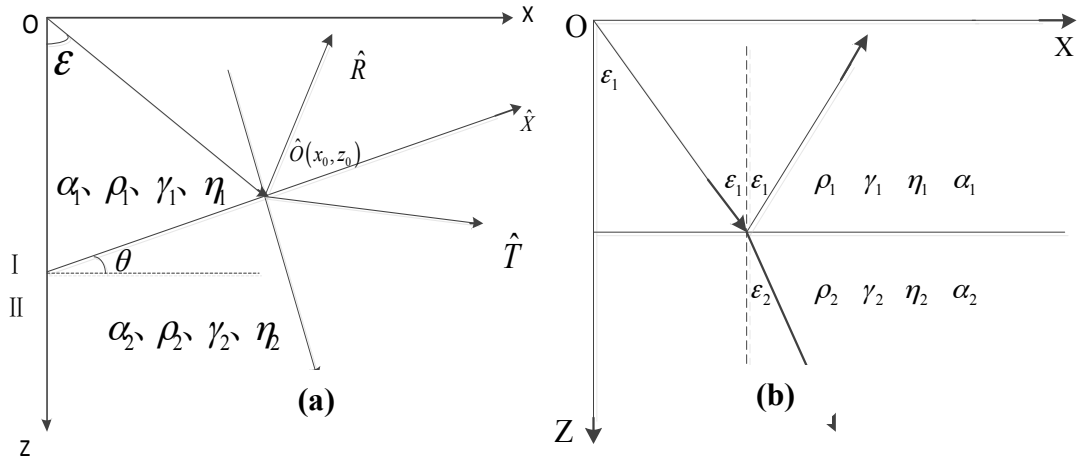

Fig. 1. The propagation of the plane wave in the diffusive-viscous media with a single interface. (a) Two layered diffusive-viscous media with a dipping interface in the global system. (b) Two layered diffusive-viscous media with a horizontal interface in the local system.

First, the downgoing incident wave in the global system is written as

$$\phi_1 = \exp\left[j\omega\left(p_1 x + q_1 z\right)\right], \tag{6}$$

where the time factor $e^{j\omega t}$ has been suppressed, p_1 and q_1 are the horizontal and vertical slownesses in the global coordinate system, respectively.

Because the wave propagation is independent of coordinate systems, the simplified equations of incident wave in the local system can be obtained by replacing (x, z) with $(\hat{x}, \hat{z})$ as eqs. (7) and (8)

$$\hat{\phi}_1 = \exp\left[j\omega\left(p_1 x_0 + q_1 z_0\right)\right]\exp\left[j\omega\left(\hat{p}_1\hat{x} + \hat{q}_1\hat{z}\right)\right], \tag{7}$$

$$\begin{bmatrix} p_1 \\ q_1 \end{bmatrix} = \mathbf{C}^{-1}\begin{bmatrix} \hat{p}_1 \\ \hat{q}_1 \end{bmatrix}, \tag{8}$$

where the superscript "∧" indicates that relative variables are discussed in the local coordinate system. $\hat{p}_1$ and $\hat{q}_1$ are the horizontal and vertical slowness in the local coordinate system, respectively.

In the local coordinate system, the dipping interface is considered as horizontal, which separates two diffusive-viscous media as shown in Fig. 1(b). The secondary waves in both half-spaces can be written as

$$\hat{\psi}_2 = \hat{T}^d \cdot \exp\left[j\omega\left(p_1 x_0 + q_1 z_0\right)\right] \cdot \exp\left[j\omega\left(\hat{p}_2\hat{x} + \hat{q}_2\hat{z}\right)\right], \tag{9}$$

$$\hat{\varphi}_1 = \hat{R}^d \cdot \exp\left[j\omega\left(p_1 x_0 + q_1 z_0\right)\right] \cdot \exp\left[j\omega\left(\hat{p}_1\hat{x} - \hat{q}_1\hat{z}\right)\right], \tag{10}$$

where $\hat{R}^d$ and $\hat{T}^d$ denote the reflection and transmission coefficients corresponding to the downgoing-waves in the local coordinate system. The subscript "2" represents that parameters are in the second layer. Boundary conditions require that the pressure and particle velocity projection on the normal of the boundary are continuous. The reflection and transmission coefficients can be written as

$$\hat{R}^d = \frac{\rho_2\hat{q}_1 - \rho_1\hat{q}_2}{\rho_2\hat{q}_1 + \rho_1\hat{q}_2}, \tag{11}$$

$$\hat{T}^d = \frac{2\rho_1\hat{q}_2}{\rho_2\hat{q}_1 + \rho_1\hat{q}_2}. \tag{12}$$

In acoustic media, the vertical slowness is always real. Although eqs. (11) and (12) have the same form as in case of acoustic media, the slownesses and the coefficients are complex and dependent on frequency. The question is how to correctly choose the sign of the vertical slownesses in eqs. (11) and (12) to avoid the instability in wave propagation. In this paper, we choose the imaginary part of the vertical slowness related to the downgoing- and upgoing- waves as positive and negative, respectively.

Substituting $(\hat{x},\hat{z})$ with (x,z) in eqs. (9) and (10), the secondary waves in the global coordinate system become

$$\psi_2 = \hat{T}^d \cdot \exp\left[j\omega\left(p_1x_0 + q_1z_0\right)\right] \cdot \exp\left[j\omega\left(-p_2x_0 - q_2z_0\right)\right] \cdot \exp\left[j\omega\left(p_2x + q_2z\right)\right], \tag{13}$$

$$\varphi_1 = \hat{R}^d \cdot \exp\left[j\omega\left(p_1x_0 + q_1z_0\right)\right] \cdot \exp\left[-j\omega\left(p_1x_0 - q_1z_0\right)\right] \cdot \exp\left[j\omega\left(p_1x - q_1z\right)\right], \tag{14}$$

$$\begin{bmatrix} p_2 \\ q_2 \end{bmatrix} = \mathbf{C}^{-1} \begin{bmatrix} \hat{p}_2 \\ \hat{q}_2 \end{bmatrix}. \tag{15}$$

We consider the reflection and transmission coefficients R^d and T^d in the global coordinate system as

$$R^d_{pp} = \hat{R}^d_{pp} \cdot \exp\left[j\omega\left(p_1x_0 + q_1z_0\right)\right], \tag{16}$$

$$T^d = \hat{T}^d \cdot \exp\left[j\omega\left(p_1x_0 + q_1z_0\right)\right]. \tag{17}$$

So eqs. (13) and (14) can be re-written as

$$\psi_2 = T^d \cdot \exp\left[j\omega\left(p_2\left(x - x_0\right) + q_2\left(z - z_0\right)\right)\right], \tag{18}$$

$$\varphi_2 = R^d \cdot \exp\left[j\omega\left(p_1\left(x - x_0\right) - q_1\left(z - z_0\right)\right)\right], \tag{19}$$

For transmitted waves, we have

$$\psi_1 = T^u \cdot \exp\left[j\omega\left(p_1\left(x - x_0\right) - q_1\left(z - z_0\right)\right)\right], \tag{20}$$

$$T^u = \hat{T}^u \cdot \exp\left[j\omega\left(p_2 x_0 - q_2 z_0\right)\right], \tag{21}$$

$$\begin{bmatrix} p_1 \\ q_1 \end{bmatrix} = \mathbf{C} \begin{bmatrix} \hat{p} \\ \hat{q}_1 \end{bmatrix}, \tag{22}$$

$$\begin{bmatrix} p_2 \\ q_2 \end{bmatrix} = \mathbf{C}^{-1} \begin{bmatrix} \hat{p}_2 \\ \hat{q}_2 \end{bmatrix}, \tag{23}$$

where the superscript "u" denotes that the variables are corresponding to the upgoing-waves. The multiple components can be calculated in the same way. The proposed method can simulate different wave components. Meanwhile, the proposed method is valid when interfaces are horizontal. The coefficients of secondary waves at dipping interfaces in the global coordinate system depend on the position and dipping angles of interfaces. The ray slowness is not conserved in layered media with dipping interfaces.

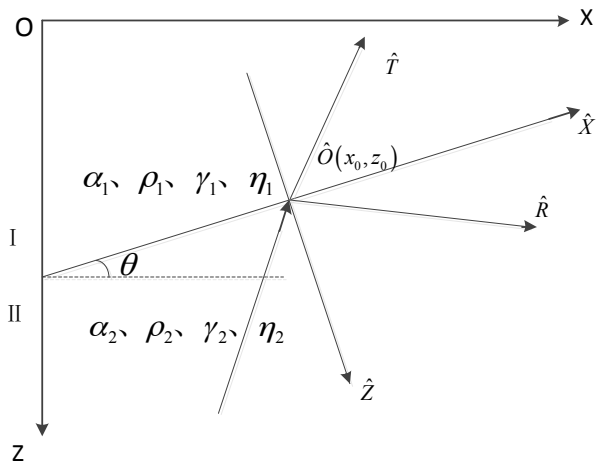

Fig. 2. Two half-spaces with a dipping interface. For an upgoing plane wave, there are two secondary waves.

PARTIAL WAVE PROPAGATION IN LAYERED MEDIA

We consider a layered medium with dipping interfaces shown in Fig. 3. The position of a point source is placed at the origin in the global coordinate system. To construct the local coordinate system, each interface is considered along the $\hat{X}$-axis of the local coordinate system.

The incident plane waves in the global coordinate system are shown in eq. (6). The complete modeling procedure is shown in Fig. 4.

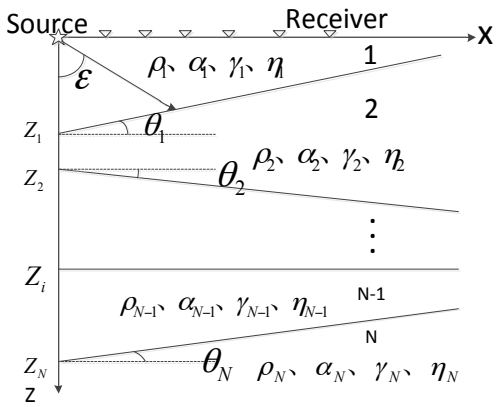

Fig. 3. The wave propagation in a layered diffusive-viscous media.

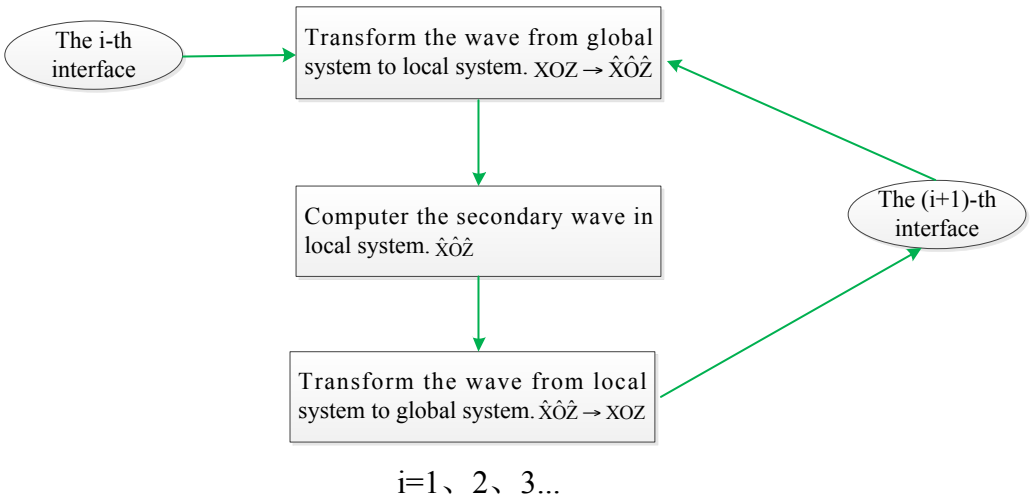

Fig. 4. The recursion procedure for layered media. (1) Constructing a local coordinate system $\hat{X}\hat{O}\hat{Z}$ for the i-th interface. The origin of the local coordinate system (x_{i-1}, z_{i-1}) in the global plane could be given anywhere. (2) The wave equations in XOZ system are transformed into $\hat{X}\hat{O}\hat{Z}$ system. Then, the specific simulation process as shown in Fig. 1 and Fig. 2 is introduced to calculate the reflected wave and transmitted wave which are in XOZ system. (3) Iterating the step 1 and step 2 layer by layer.

The equation of primary downgoing-waves in the layer i is

$$\psi_i = \prod_{n=1}^{i} T_n^d \exp\left[j\omega\left(p_i\left(x - x_{i-1}\right) + q_i\left(z - z_{i-1}\right)\right)\right], i = 1,2,3\mathrm{K}\ N. \tag{24}$$

The transmission coefficient at the dipping interface in the global coordinate system is

$$T_{pp\cdot n}^d = \hat{T}_{pp\cdot n}^d \exp\left[j\omega\left(p_{np}\left(x_{n-1} - x_{n-2}\right) + q_{np}\left(z_{n-1} - z_{n-2}\right)\right)\right], n = 1,2,3\mathrm{L}\ N \tag{25}$$

where (x_{i-1}, z_{i-1}) represents the source at the origin of the global coordinate system. In eqs. (24) and (25), points (x_i , z_i) are the origins of the local coordinate system in the global coordinate system.

There are some recursive relations, defined in eqs. (26), (27) and (28).

$$\mathbf{C}_{i-1} = \begin{bmatrix} \cos\theta_{i-1} & \cos\theta_{i-1} \\ -\sin\theta_{i-1} & \cos\theta_{i-1} \end{bmatrix}, i = 2,3,4\mathrm{L}\ \ N \tag{26}$$

$$\hat{p}_i = \hat{p}_{i-1}, \hat{q}_i = \sqrt{\alpha_i^{-2} - \hat{p}_i^2}, \tag{27}$$

$$\begin{bmatrix} p_i \\ q_i \end{bmatrix} = \mathbf{C}_{i-1}^{-1} \begin{bmatrix} \hat{p}_i \\ \hat{q}_i \end{bmatrix}, \tag{28}$$

where θ_{i-1} is the dipping angle of the interface between the layer $i-1$ and layer i.

The primary reflection wave in the layer m reflected from the interface i is

$$\phi_{m,i} = \prod_{n=0}^{i-1} T_n^d \cdot R_i^d \cdot \prod_{m=0}^{i-1} T_m^u \cdot \exp\left[j\omega\left(p_m\left(x - x_{m-1}\right) - q_m\left(z - z_{m-1}\right)\right)\right], i = 1,2\mathrm{L} \tag{29}$$

where T_m^u denotes the transmission coefficient corresponding to the upgoing-wave at m-th interface. R_i^d is the reflection coefficient corresponding to the downgoing-wave at i-th interface. T_n^d is the transmission coefficient corresponding to the downgoing-wave at n-th interface. At the free surface, $T_0^u = 1$ and $T_0^d = 1$.

To study waves that we are interested, raytracing method of Cerveny (2005) is used. The code procedure is that "+" represents downgoing-waves and "−" represents the upgoing-waves. A four-dimensional code [+, +, -, -] represents the wave propagation shown in Fig. 5. For different waves in media with multiple layers, the modeling procedure can be coded as multi-dimension.

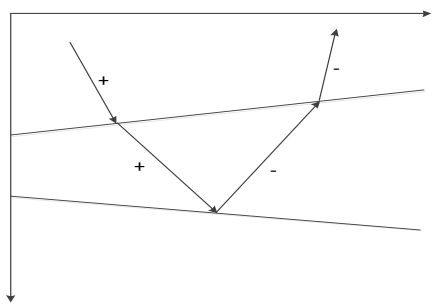

Fig. 5. Wave propagation of the code [+, +, -, -].

SYNTHESIZING RECORDING OF A POINT SOURCE

Synthetic seismograms for a point source can be calculated by a superposition of all plane waves (Aki and Richards, 2002). Here, we introduce a slowness integral

$$W=\frac{1}{2\pi}\cdot\int_{\Gamma} f\left(p_s\right)\cdot\frac{\exp\left[j\omega\left(p_r x\pm q_r z\right)\right]}{-2jq_s}dp_s. \tag{30}$$

Eq. (30) is an integral formula about the horizontal slowness. p_s and q_s represent the horizontal and vertical slownesses of plane waves at the source. p_r and q_r are the slownesses of reflection waves at receivers. $f\,(p_s)$ is the reflection coefficient (or the transmission coefficient). Γ represents the integral contour of the horizontal slowness in a complex plane.

For primary reflected waves from all interfaces in media as shown in Fig. 3, the synthetic wavefield can be written as

$$W_p=\frac{1}{2\pi}\cdot\int_{\Gamma}\sum_{i=1}^{N-1}R_i\left(p_s\right)\cdot\frac{\exp\left[j\omega\left(p_r x-q_r z\right)\right]}{-2jq_s}dp_s, \tag{31}$$

$$R_i\left(p_s\right)=\prod_{n=0}^{i-1}T_n^d\cdot R_i^d\cdot\prod_{m=0}^{i-1}T_m^u. \tag{32}$$

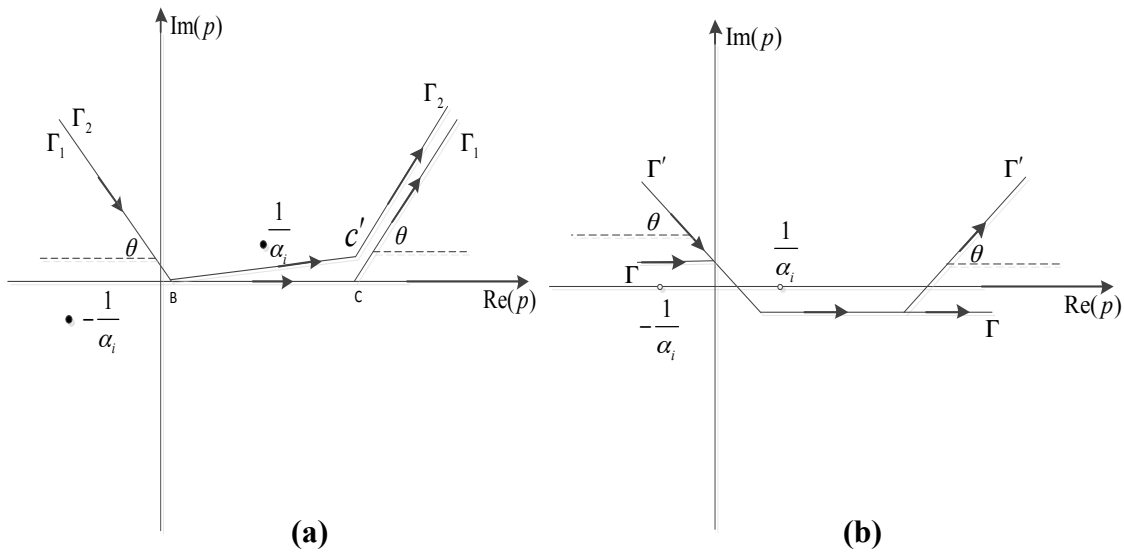

Fig. 6. The integral contour of horizontal slowness in the complex plane. θ is the angle between Γ and the real axis, α_i is the wave velocity. (a) The integral paths for elastic media, which are deviated from the real axis slightly to avoid the poles at the real axis. (b) The integral paths for diffusive-viscous media.

According to the residue theorem, many integral paths can be chosen from a complex plane. In elastic media, the integral path Γ is along the real axis. To avoid poles at the real axis, the integral path is usually deviated from the real axis slightly, shown Fig. 6(a) (Fuchs and Müller, 1971; Chapman, 1978). Frazer and Gettrust (1984) introduced the integral path Γ' shown in Fig. 6(a). For a single receiver, the integral has a fast convergence rate when $\theta = \tan^{-1}\left(x/|z_r - z_s|\right)$, where x is the offset, z_r and z_s are the receiver and source positions along the Z axis, respectively. In the case of attenuation, the integral path can be chosen as the real axis due to the poles in the first and third quadrants, it can also reduce the complexity of the computation. We choose the integral path Γ_1 shown in Fig. 6(b), and synthesis seismograms are shown in Fig. 7(a). However, the section BC of the integral path Γ_1 along the real axis is dominant of eq. (31). It indicates that there is no attenuation when the wave propagates along horizontal directions. The integral path Γ_1 is modified to the path Γ_2. There is a small angle, between segment BC and real axis, ensure the segment BC' is slightly below the poles. Synthesis seismogram is shown in Fig. 7(b). The comparison of the peak amplitude of synthetic seismograms with the paths Γ_1 and Γ_2 is shown in Fig. 7(c).

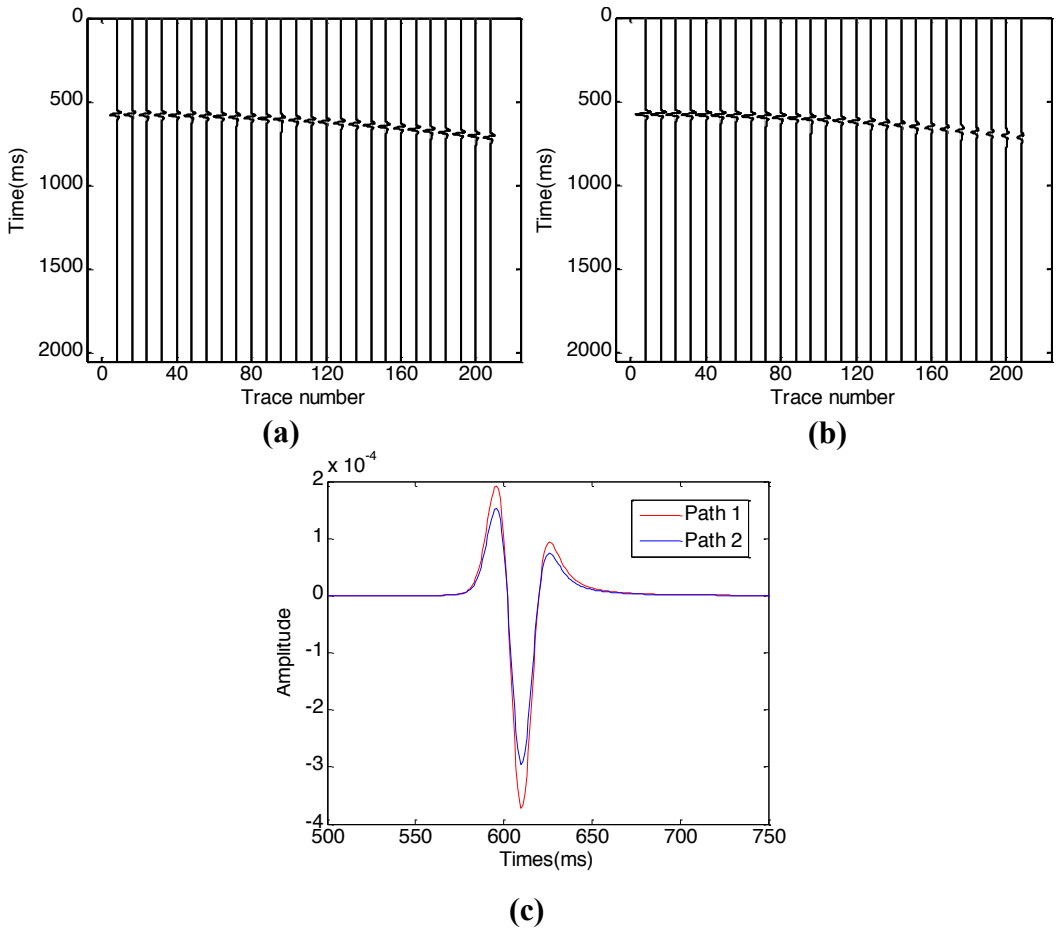

Fig. 7. The synthesis seismograms of diffusive-viscous which are calculated by the different integral path shown in Fig. 6(b). (a) The synthesis seismogram calculation by path Γ_1. (b) The synthesis seismogram calculation by path Γ_2. (c) The comparison for the peak amplitude of the synthetic seismograms with the path Γ_1 and Γ_2.

For the oscillatory integral shown in eq. (31), there are classic computation methods, such as the standard trapezoidal method, the Filon's method (FM) (Filon, 1930), the generalization of Filon's method (GFM) (Frazer and Gettrust, 1984), and the Hermite interpolation method. In practice, we can choose an appropriate method according to the kernel functions of oscillatory integrals. In the reflectivity integral computations, the GFM approach is more efficient than non-Filon quadrature technique (Frazer and Gettrust, 1984). According to the GFM, the slowness integral can be rewritten in the form of $\int f(p)\exp[sg(p)]dp$ as

$$f(p)=\frac{-R_i(p_s)}{2\pi\cdot 2jq_s},\quad s=j\omega\max(x,z),\quad g(p)=\frac{p_r x-q_r z}{\max(x,z)}. \tag{33}$$

The GFM analogue of the trapezoidal rule is

$$\int_{p1}^{p2} f(p)\exp[sg(p)]dp=\begin{cases}\dfrac{D(p)}{sD(g)}\left[D[f\exp(sg)]-\dfrac{D(f)D[\exp(sg)]}{sD(g)}\right] & D(g)\neq 0\\ \dfrac{D(p)}{2}\quad[f_1\exp(sg_1)+f_2\exp(sg_2)]\exp(sg_1) & D(g)=0\end{cases}, \tag{34}$$

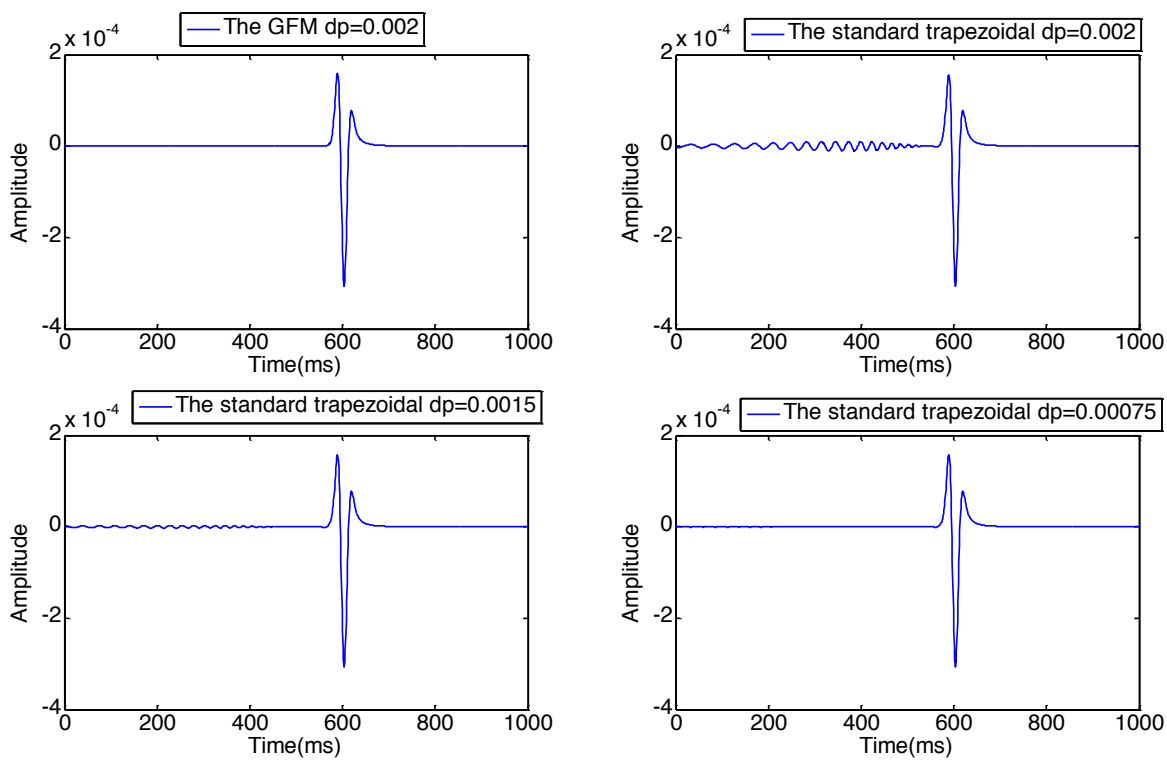

Fig. 8. The comparison of the accuracy of the quadrature which is calculated by GFM and the standard trapezoidal, respectively.

where $p2-p1$ is the integral step. Note that $p2-p1$ is the inversely proportional to $\sqrt{\max(\omega x,\omega z)}$. The specification operator $D(h)$ indicates $h(p2)-h(p1)$ for any function $h(p)$. Fig. 8 shows the comparison of the GFM and the standard trapezoidal method for the same diffusive-viscous model, we can see that the GFM obtains accurate results when the integration step $dp=0.002$. In contrast, the result of the standard trapezoidal is not as accurate as the GFM due to oscillation as it needs smaller step size.

NUMERICAL EXAMPLES

In this section, we synthesize seismograms from several models using our method. For comparison, the synthetic seismograms are also compared with the results from the Flux-Corrected Transport-Finite-Difference method (FCT-FDM). The FCT-FDM was first introduced to model propagations of diffusive-viscous waves by Zhao (2014).

To verify the validity of the proposed method and to illustrate the diffusive-viscous attenuation effects, the first theoretical model with a thin plane bed sandwiched between two homogeneous half-spaces is chosen, shown in Fig. 9(a). The parameters are given in Table 1. We consider three cases in this model: standard acoustic case, viscoelastic case and diffusive-viscous case. For the same layer in different cases, we only modify the attenuation parameters, and all the other parameters keep invariable. The time sampling rate is 1 ms. A Ricker wavelet with a dominate frequency of 40 Hz is placed at the origin $(0,0)$, and has a 100 ms time-delay.

In Figs. 9(b) and 9(c), the reflection wavefields have some substantial differences between water-saturated layers and dry-sandstone layer. The water-saturated layers cause a noticeable time delay in waveforms and the loss of high-frequency energy. It is clear that there is a less obvious time delay in Figs. 9(d) to 9(e) for thin beds with dry-sandstone. However, the energy redistributions between different frequencies are observed due to the introduction of diffusive-viscous parameters. Figs. 9(f) and 9(g) show that the same phenomenon can be seen as Fig. 9(d) and 9(e). From this comparison, we see that the diffusive-viscous parameters can explain the observation of Korneev et al. (2004).

To verify the validity of the proposed method for diffusive-viscous media with dipping interfaces, the second test model is presented as shown in Fig. 10(a). The dipping angles of the upper interface and the lower interface are 15 and 10 degrees, respectively. The distance between receivers is 5 m and synthetic seismograms are extracted every 8 traces. The half-spaces parameters are the same as those shown in Table 1 and the thin layer is water-saturated. Figs. 10(b) and 10(c) show that synthetic seismogram contains all primary reflected waves and the interfaces cannot be distinguished. As a result, the presence of thin layers cannot be identified. All the partial waves can be modeled as shown using the proposed method in this paper as shown in Fig. 10.

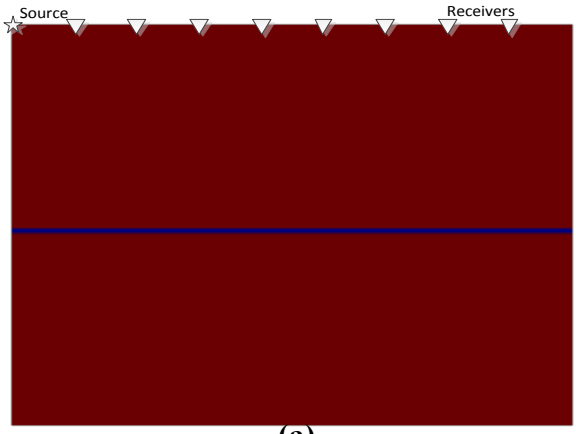
Source
Receivers

(a)

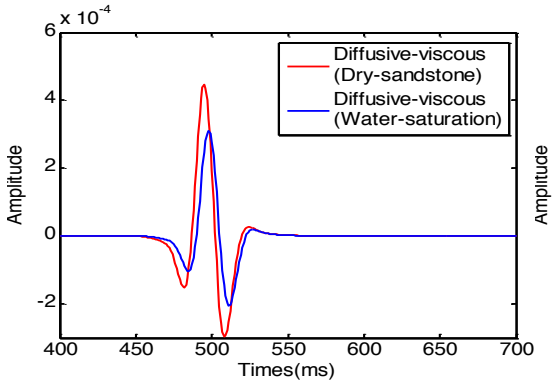
x 10^-4
Amplitude
Times(ms)
Diffusive-viscous (Dry-sandstone)
Diffusive-viscous (Water-saturation)

(b)

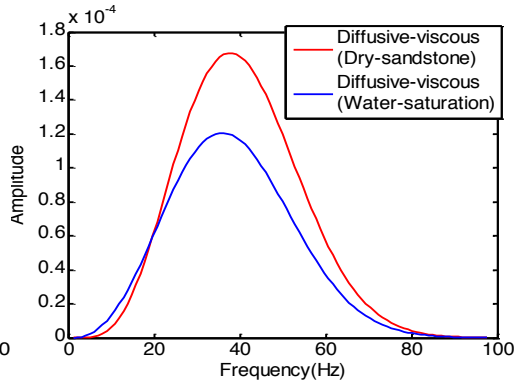
x 10^-4
Amplitude
Frequency(Hz)
Diffusive-viscous (Dry-sandstone)
Diffusive-viscous (Water-saturation)

(c)

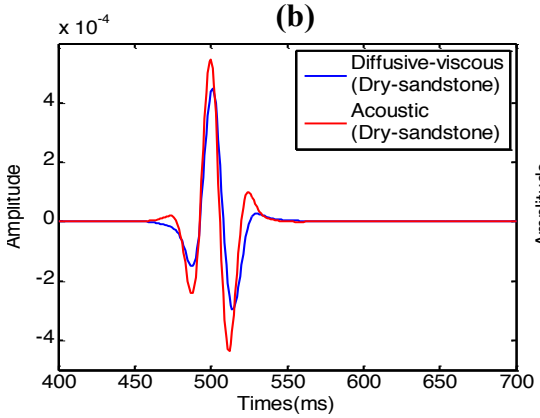
x 10^-4
Amplitude
Times(ms)
Diffusive-viscous (Dry-sandstone)
Acoustic (Dry-sandstone)

(d)

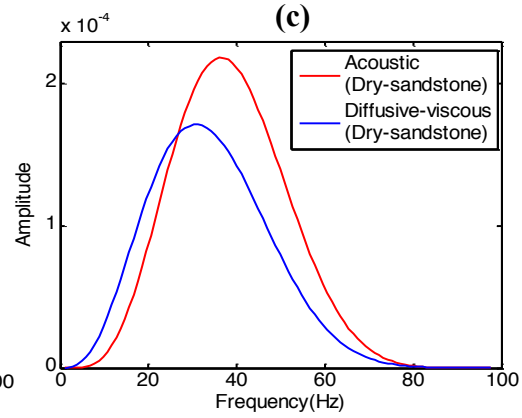
x 10^-4
Amplitude
Frequency(Hz)
Acoustic (Dry-sandstone)
Diffusive-viscous (Dry-sandstone)

(e)

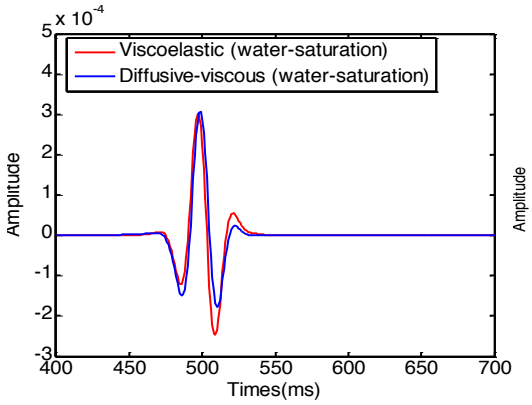
x 10^-4
Amplitude
Times(ms)
Viscoelastic (water-saturation)
Diffusive-viscous (water-saturation)

(f)

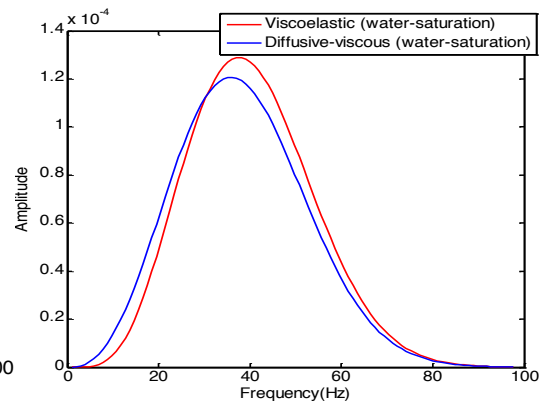
x 10^-4
Amplitude
Frequency(Hz)
Viscoelastic (water-saturation)
Diffusive-viscous (water-saturation)

(g)

Fig. 9. (a) A three-layered media with horizontal interfaces and the thin layer is 10 m thickness. The integral interval of horizontal slowness is $\left[-1/v_1, 1/v_1\right]$ and the integral step is 0.0025s/m. (b) The comparison of the reflection waves in the time domain between the dry-sandstone layer and the water-saturation layer based on diffusive-viscous theory. (c) The comparison of the reflection waves in the frequency domain between the dry-sandstone layer and the water-saturation layer based on diffusive-viscous theory. (d) The comparison of the reflection waves in the time domain between the diffusive-viscous case and the acoustic case ($\gamma=\eta=0$), both them are a dry-sandstone layer. (e) The comparison of the reflection waves in the frequency domain between the diffusive-viscous case and the acoustic case, both them are a dry-sandstone layer. (f) The comparison of the reflection waves in the time domain between the diffusive-viscous case and the viscoelastic case ($Q=16$), both them are a water-saturation layer. (g) The comparison of the reflection waves in the frequency domain between the diffusive-viscous case and the viscoelastic case, both them are a water-saturation layer.

Table1. The parameters of the fluid-saturated sandstone medium for Figs. 9(a) and 10(a).

Layers	$\rho\left(g\cdot cm^{-3}\right)$	$v\left(m/s\right)$	$\gamma\left(Hz\right)$	$\eta\left(m^2/s\right)$	Thickness (m)
Half space	1.2	2300	0.0001	0.0001	450
Dry-sandstone	1.8	1190	56	0.056	10
Water-saturation	2.1	1470	90	0.2	10

CONCLUSIONS

In this paper, we proposed an efficient partial wavefield modeling method in layered diffusive-viscous media with dipping interfaces. The synthetic seismograms compared with the finite difference method show that the proposed method is computationally efficient and can be used to model thin layers. The synthetic seismogram of a particular wavefield can be used to help us to investigate seismic characteristics of thin layers. After showing the application of the method to model primary reflection waves, we believe it can be applied to model multiples. In summary, our study aims to understand the wave propagation in fluid-saturated media and explain the physical phenomena associated with the characteristics of porous media. These results would be useful to help interpret field data and contribute to the fluid identification. However, the proposed method cannot be considered as the optimal method in all cases, such as the presence of fractures or with complex structures. The proposed method can be seen as an extension of the reflectivity method for diffusive-viscous media with horizontal or dipping layers. The main limitation is that it cannot be applied to the case where the downgoing reflections are excited from the downgoing incident waves, because dipping interfaces are too steep. Dipping angles should be limited in an appropriate range to avoid the downgoing reflections. Note that the physical interpretation of diffusion–dissipation term remains to be understood. Korneev et al. (2004) speculate that the fluid flow in the matrix can be the main driving mechanism of fluid diffusion-dissipation.

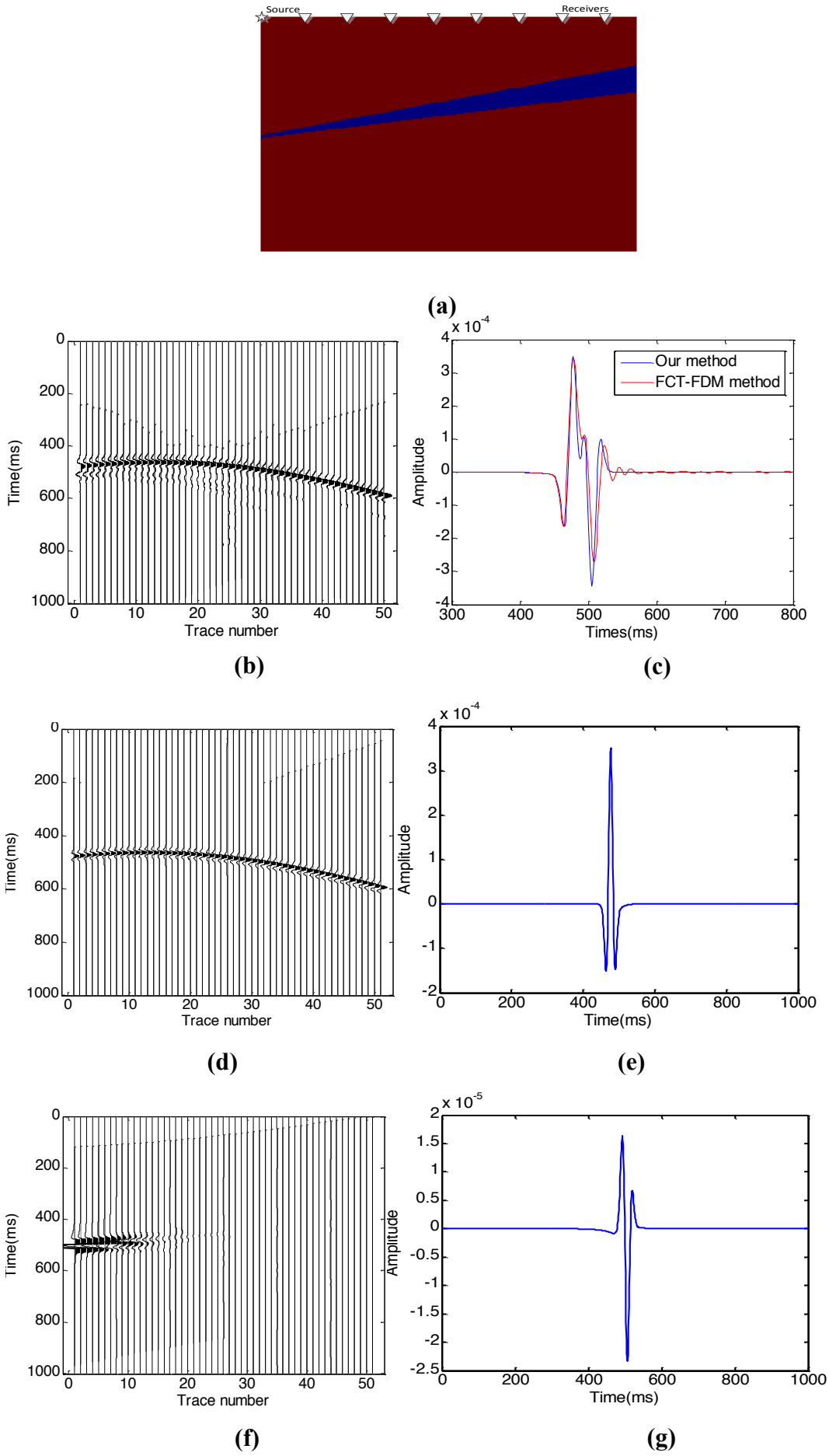
Source
Receivers
(a)
Time(ms)
Trace number
(b)
x 10^-4
Our method
FCT-FDM method
Amplitude
Times(ms)
(c)
Time(ms)
Trace number
(d)
x 10^-4
Amplitude
Time(ms)
(e)
Time(ms)
Trace number
(f)
x 10^-5
Amplitude
Time(ms)
(g)

Fig. 10. (a) The second theoretical model which is a descendant from the first model Fig.9(a). The dipping angles for the upper interface and the lower interface are 15,10 degrees, respectively. The other parameters remain unchanged. The integral interval of horizontal slowness is $\left[-1/v_1, 1/v_1\right]$ and the integral step is 0.002 s/m. (b) The comparison of synthetic seismogram calculated by our method and by Flux-Corrected Transport-Finite-Difference method (FCT-FDM). (c) The comparison of the first trace in the synthetic seismogram. (d) The primary reflected waves that are reflected by the upper interface. (e) The first trace reflected by the upper interface. (f) The primary reflected waves that are reflected by the lower interface. (g) The first trace reflected by the lower interface.

ACKNOWLEDGEMENTS

We thank the editor, the reviewer Dr. Enru Liu and the other anonymous reviewers for reviewing this manuscript. They provided insightful suggestions that greatly improve the quality of this paper. We thank the financial support from the following programs: the National Natural Science Foundation of China (41390450, 41390454) and the National Science and Technology Major Project (2016ZX05024-001-007, 2017ZX05069).

REFERENCES

Alterman, Z. and Karal, F.C., 1968. Propagation of elastic waves in layered media by finite difference methods. Bull. Seismol. Soc. Am., 58: 367-398.

Arntsen, B., Nebel, A.G. and Amundsen, L., 1998. Viscoacoustic finite-difference modeling in the frequency domain. J. Seismic.Explor., 7: 45-64.

Aki, K. and Richards, P.G., 2002. Quantitative Seismology. W.H. Freeman, San Francisco.

Berkhout, A.J., Ridder, J. and van der, Wal, L.F., 1982. Acoustic Imaging by Wave Field Extrapolation Part I: Theoretical Considerations. Acoustical Imaging. Springer, New York: 513-540.

Bourbie, T. and Gonzalez-Serrano, A., 1983. Synthetic seismograms in attenuating media. Geophysics, 48: 1575-1587.

Chapman, C.H., 1978. A new method for computing seismograms. Geophys. J. Internat., 54: 481-518.

Chen, X.F., 1990. Seismogram synthesis for multi-layered media with irregular interfaces by global generalized reflection/transmission matrices method. I. Theory of two-dimensional SH case. Bull. Seismol. Soc. Am., 80: 1696-1724.

Chen, X.F., 1996. Seismogram synthesis for multi-layered media with irregular interfaces by global generalized reflection/transmission matrices method. III. Theory of 2D P-SV case. Bull. Seismol. Soc. Am., 86: 389-405.

Carcione, J.M. and Tinivella, U., 2001. The seismic response to overpressure: a modeling study based on laboratory, well and seismic data. Geophys. Prosp., 49: 523-539.

Cerveny, V., 2005. Seismic Ray Theory. Cambridge University Press, Cambridge.

Filon, L.N.G., 1930. III—On a quadrature formula for trigonometric integrals. P. Roy. Soc. Edinb. A., 49: 38-47.

Fuchs, K. and Müller, G., 1971. Computation of synthetic seismograms with the reflectivity method and comparison with observations. Geophys. J. Int., 23: 417-433.

Frazer, L.N. and Gettrust, J.F., 1984. On a generalization of Filon's method and the computation of the oscillatory integrals of seismology. Geophys. J. Internat., 76: 461-481.

Goloshubin, G.M., Verkhovsky, A.M., and Kaurov, V.V., 1996. Laboratory experiments of seismic monitoring. Extended Abstr., 58th EAGE Conf., Amsterdam.

Guo, H.Y., Xiao-Mei, J.I. and Yu-Qi, L.I., 2001. A note on symplectic, multisymplectic scheme in finite element method. Commun. Theor. Phys., 36: 259-262.

Ge, Z. and Chen, X., 2007. Wave propagation in irregularly layered elastic models: a boundary element approach with a global reflection/transmission matrix propagator. Bull. Seismol. Soc. Am., 97: 1025-1031.

Gao, J. and Zhang, Y., 2013. Staggered-grid finite difference method with variable-order accuracy for porous media. Math. Probl. Engin., Article ID 157071, 1-10.

Han, B., He, Q., Chen, Y. and Dou, Y., 2014. Seismic waveform inversion using the finite-difference contrast source inversion method. J. Appl. Math., Article ID 532159, 1-11.

ten Kroode, F., 2002. Prediction of internal multiples. Wave Motion., 35: 315-338.

Korneev, V.A., Goloshubin, G.M. and Daley, T.M., 2004. Seismic low-frequency effects in monitoring fluid-saturated reservoirs. Geophysics, 69: 522-532.

Liu, E., Zhang, Z.J., Yue, J.H. and Dobson, A., 2008. Boundary Integral Modelling of Elastic Wave Propagation in Multi-Layered 2D Media with Irregular Interfaces. Commun. Comput. Phys., 3: 52-62.

Marfurt, K.J., 1984. Accuracy of finite-difference and finite-element modeling of the scalar and elastic wave equations. Geophys., 49: 533-549.

Mars, J., Iii, R., James, W. and Lazaratos, S.K., 1999. Filter formulation and wavefield separation of cross-well seismic data. Geophys. Prosp., 47: 611-636.

Min, D.J., 2002. Weighted-averaging finite-element method for 2d elastic wave equations in the frequency domain. J. Seis. Explor., 5: 197-222.

Meng, W. and Fu, L.Y., 2017. Seismic wavefield simulation by a modified finite element method with a perfectly matched layer absorbing boundary. J. Geophys. Engin., 14: 852-864.

Nowak, E.J. and Imhof, M.G., 2004. Diffractor localization via weighted Radon transforms. Expanded Abstr., 74th Ann. Internat. SEG Mtg., Denver: 2108-2111.

Patera, A.T., 1984. A spectral element method for fluid dynamics: laminar flow in a channel expansion. J. Comput. Phys., 54: 468-488.

Raikes, S.A. and White, J.E., 1984. Measurements of earth attenuation from downhole and surface seismic recording. Geophys. Prosp., 32: 892-919.

Peelamedu, S.M., 1999. Active strain transfer analysis in a piezoceramic system using finite element method and experimental investigation. Smart Mater. Struct., 8: 654.

Smith, W.D., 1975. The application of finite element analysis to body wave propagation problems. Geophys. J. Internat., 42: 747-768.

Shuey, R.T., 1985. A simplification of the Zoeppritz equations. Geophysics, 50: 609-614.

Serdyukov, A.S. and Duchkov, A., 2015. Hybrid Kinematic-dynamic approach to seismic wave equation modeling, imaging, and tomography. Math. Probl. Eng., Article ID 543540, 1-8.

Toksöz, M.N. and Johnston, D.H., 1981. Seismic Wave Attenuation. SEG, Tulsa, OK.

Taeyoung, H., Yunseok, C., Shin, C. and Min, D.J., 2009. Numerical modeling for 3D acoustic wave equation in the frequency domain. J. Seismic Explor., 18: 57-79.

Wu, C. and Harris, J. M., 2004. An optimized variable-grid finite-difference method for seismic forward modeling. J. Seismic Explor., 12: 343-353.

Wang, M., Hung, B., Li, X. and Fintz, S., 2016. Challenges and strategies of interbed multiple attenuation in the Asia-Pacific region. Geophys. Prosp., 34: 81-85.

Zhang, F. and Li, X., 2013. Generalized approximations of reflection coefficients in orthorhombic media. J. Geophys. Engin., 10: 054004.

Zhao, H., Gao, J. and Zhao, J., 2014. Modeling the propagation of diffusive-viscous waves using flux-corrected transport–finite-difference method. IEEE J-Stars., 7: 838-844.

Zhao, H.X., Gao, J.H. and Peng, J.G., 2017. Extended reflectivity method for modeling the propagation of diffusive-viscous wave in dip-layered media. Geophys. Prosp., 65: 4018-4022.

APPENDIX

We start from the stress-strain relation:

$$\sigma(t) = M(t)\varepsilon(t). \tag{A-1}$$

In eq. (A-1), σ denotes the stress and M is the complex modulus, ε is the strain. The Fourier transform of equation (A.1) is

$$\sigma(\omega) = M(\omega)\varepsilon(\omega). \tag{A-2}$$

The complex velocity and the quality factor can be written as

$$V = \sqrt{\frac{M}{\rho}}, \tag{A-3}$$

$$Q(\omega) = \frac{M_{re}(\omega)}{M_{im}(\omega)}, \tag{A-4}$$

where $M_{re}(\omega)$ and $M_{im}(\omega)$ are the real and imaginary parts of complex modulus $M(\omega)$. We assume the plane wave solution of the eq. (1) as

$$u\left(x,\omega\right)=u_0\left(\omega\right)\exp\left[i\left(\omega t-\tilde{k}x\right)\right], \tag{A-5}$$

where k is the complex wavenumber. From eqs. (A-5), (A-1), (A-3) and (A-4), we can obtain

$$V^2=\frac{\omega^2}{\tilde{k}^2}, \tag{A-6}$$

$$M=\frac{\rho\omega^2}{\tilde{k}^2}, \tag{A-7}$$

$$Q\left(\omega\right)=\frac{M_{re}}{M_{im}}=\frac{\mathrm{Re}\left(\dfrac{\omega^2}{\tilde{k}^2}\right)}{\mathrm{Im}\left(\dfrac{\omega^2}{\tilde{k}^2}\right)}=\frac{\mathrm{Re}\left(V^2\right)}{\mathrm{Im}\left(V^2\right)}. \tag{A-8}$$